Pinning-Free Evaporation of Sessile Droplets of Water from Solid Surfaces

Steven Armstrong, Glen McHale, Rodrigo Ledesma-Aguilar and Gary G. Wells

Smart Materials & Surfaces Laboratory, Faculty of Engineering & Environment,

Northumbria University, Newcastle upon Tyne, UK

Corresponding Author: glen.mchale@northumbria.ac.uk

Abstract

Contact-line pinning is a fundamental limitation to the motion of contact lines of liquids on solid surfaces. When a sessile droplet evaporates, contact-line pinning typically results in either a stick-slip evaporation mode, where the contact line pins and de-pins from the surface in an uncontrolled manner or a constant contact area mode with a pinned contact line. Pinning prevents the observation of the quasi-equilibrium constant contact angle mode of evaporation, which has never been observed for sessile droplets of water directly resting on a smooth, non-textured, solid surface. Here, we report the evaporation of a sessile droplet from a flat glass substrate treated with a smooth, Slippery Omni-phobic Covalently Attached Liquid-like (SOCAL) coating. Our characterization of the surfaces shows a high contact line mobility with an extremely low contact angle hysteresis of ~1°, and reveals a step change in the value of the contact angle from 101° to 105° between a relative humidity of 30% and 40%, in a manner reminiscent of the transition observed in a type V adsorption isotherm. We observe the evaporation of small sessile droplets in a chamber held at a constant temperature, T=(25.0 ± 0.1) °C and at constant relative humidity (RH) across the range RH=10-70%. In all cases a constant contact angle mode of evaporation is observed for most of the evaporation time. Furthermore, we analyze the evaporation sequences using the Picknett & Bexon ideal constant contact angle mode for diffusion-limited evaporation. The resulting estimate for the diffusion coefficient, D_E, of water vapor in air of D_E=(2.44 ± 0.48) x 10^{-5} m^2s^{-1} is accurate to within 2% of the value reported in the literature, thus validating the constant contact angle mode of the diffusion-limited evaporation model.

Keywords: Sessile droplet, evaporation, SOCAL, superhydrophobic, SLIPS

Introduction

Evaporation of liquids occurs when the atmosphere surrounding the liquid is not saturated with the vapor of the liquid[1]. It is a widely observed natural phenomenon and is important for many applications, including inkjet printing[2], fuel delivery[3] and heat exchange[4]. In these applications, droplets rest on a solid surface and this introduces two fundamental differences to how evaporation occurs compared to spherical droplets in free space far from any surface. First, the spherical symmetry for diffusion of vapor into the space around the droplet is broken by the presence of the surface. Second, droplet contact with a surface introduces contact-line pinning, which can be problematic, for example, causing non-uniform deposition of colloidal particles as in the well-known formation of coffee ring-stains[5]. Non-uniform particle deposition causes problems in a diverse range of applications, from non-uniform delivery of the active components in aerosols used in pesticides to non-uniform fluorescence in spotted microarrays[1,5–8]. Whilst, the effect on diffusion of a surface can be modelled, contact line pinning is usually an unavoidable consequence of the contact between a droplet and the surface to which it is attached.

When a droplet is in contact with a solid surface, and at thermodynamic equilibrium, the contact angle that the droplet makes with the surface, θ_e, is, in principle, determined by the interfacial tensions of the three interfaces as described by Young's law[9]

$$\cos\theta_e = \frac{\gamma_{SV} - \gamma_{SL}}{\gamma_{LV}}, \tag{1}$$

where γ_{SV} is the solid-vapor interfacial tension, γ_{SL} is the solid-liquid interfacial tension and γ_{LV} is the liquid-vapor interfacial tension. When a droplet is small compared to its capillary length $\kappa^{-1}=(\gamma_{LV}/\rho g)^{1/2}$, where ρ is the density of the liquid and g=9.81 m s^{-2}, it adopts an axisymmetric spherical cap shape when the surface is flat and smooth with no contact-line pinning. However, in practice contact-line pinning has always been observed to some extent. Picknett & Bexon provided an analytical model describing the ideal case of diffusion-limited evaporation of a sessile droplet in the absence of gravity[10]. Their analysis includes two ideal modes of evaporation[10]. The first corresponds to a Constant Contact Radius (CCR) mode, where the apparent contact angle decreases during evaporation. Since the CCR mode of evaporation requires complete pinning of the contact line, it can be achieved experimentally and has been widely studied[1]. The second mode is a constant contact angle (CCA) mode evaporation, where the contact angle is expected to retain a constant value approximating the contact angle predicted by Young's law whilst the square of the base radius of the droplet decreases linearly in time.

The observation of the CCA mode evaporation on a smooth (non-textured) flat solid surface remains elusive because it requires complete mobility of the contact line, and the roughness of ordinary flat solid surfaces always results in some contact line pinning. Contact-line pinning is quantified experimentally by the so-called contact angle hysteresis: the difference between the advancing and receding contact angles of the droplet. Instead, many experimental studies have reported a stick-slip mode of evaporation, whereby the droplet's contact line is repeatedly pinned until the force from the out-of-equilibrium contact angle increases sufficiently and a de-pinning event and rapid contact line motion occurs. Stauber *et al.* have also detailed another mode of evaporation known as stick-slide mode of evaporation, where the contact line and contact angle decrease at the same time. They provide a model to predict the lifetime of evaporating drops in stick-slide mode evaporation[11]. Recent comprehensive reviews of sessile drop evaporation are given by Erbil[1], Cazabat & Guéna[12] and Larson[13].

Attempts to experimentally observe the CCA mode of evaporation have included the use of super-hydrophobic surfaces and Slippery Liquid Infused Porous Surfaces (SLIPS), sometimes referred to as Liquid Infused Surfaces (LIS)[14,15]. Super-hydrophobic surfaces take advantage of surface texture to suspend droplets in a Cassie-Baxter state[16] on a small solid surface fraction thereby reducing the droplet-solid contact area, increasing its contact angle and reducing contact angle hysteresis[17–19]. McHale *et*

al.[20] reported the first experiments of this type using SU-8 textured surfaces with water droplets initially evaporating in CCR mode evaporation, before retreating in a step-wise fashion as the droplet jumps between micro-pillars and ultimately converting into a Wenzel state where the droplet is impaled in the texture with a completely pinned contact line[21]. Since then, many works studying evaporation on super hydrophobic surfaces and the effect of contact angle hysteresis has been reported[22–27]. In all of these studies, the surface is no longer smooth, but is textured or rough and hydrophobic, with a contact angle far from the value given by Young's law for a smooth non-textured solid surface.

A second approach to observing a CCA mode of evaporation was introduced by Guan *at al.* who used a SLIPS approach, with a lubricant oil impregnated into a hydrophobic SU-8 textured surface[28]. The lubricant oil completely coats the solid and is immiscible to water, therefore is not displaced by it. SLIPS enables droplets to slide at tilt angles of less than 1°. However, the high mobility of droplets on SLIPS arises by the replacement of the droplet-solid interface by a droplet-lubricant interface and the removal of all direct contact between the droplet and the solid. On SLIPS, contact angles and contact radii have to be interpreted as apparent contact angles and apparent contact radii from the change in slope of the droplet close to the surface. Guan *et al.* were able to observe the pinning-free evaporation of water droplets on SLIPS and interpret their evaporation using the Picknett & Bexon diffusion-limited model, modified for the presence of a wetting ridge of the impregnated oil which surrounds the droplet's base[28]. Ultimately, neither of these two approaches have provided observation of the evaporation of sessile droplets on flat smooth (non-textured) solid surfaces without contact line pinning. A key challenge remains the ability to remove contact line pinning during evaporation of sessile droplets from non-textured solid surfaces.

Recently, Wang & McCarthy have reported a method to create Slippery Omni-phobic Covalently Attached Liquid-like (SOCAL) surfaces with contact angle hysteresis less than 1°.[29] SOCAL surfaces use polydimethylsiloxane (PDMS) chains grafted to the substrate. The chains are flexible and have the ability to move independently of each other. This flexibility results in a completely mobile contact line on the solid that enables droplets to move across a surface with virtually no pinning. Importantly, SOCAL is a covalently attached layer, rather than a liquid coating retained by a surface texture as occurs in SLIPS. It also provides a coating that is on the nanometric scale as opposed to the micrometric scale of SLIPS, allowing for a clearly defined contact angle for a sessile droplet on the coated flat smooth solid surface. The report by Wang and McCarthy of smooth low hysteresis surfaces *via* a liquid-like coating with advancing and receding water contact angles of $\theta_A = 104.6°$ and $\theta_R = 103.6°$ and tilt angles for motion of 4.7° and 1.3° for droplet volumes of 3 and 20 μl, respectively,[29] has been noted by a range of researchers, but few have implemented the method. Jin *et al.* reported SOCAL contact angles of $\theta_A = 103.0°$ and $\theta_R = 98.2°$ on silicon substrates[30] and Mizutani *et al.* have reported grafting SOCAL to surgical diamond wheels for minimally invasive bone surgery and they also grafted SOCAL to a nickel substrate with a static contact angle $\theta_s = 94.1°$ and a sliding angle of 40°[31]. Daniel *et al.* also reported dissipative force acting on a droplet moving on several types of low hysteresis surfaces, including a SOCAL surface (prepared following the Wang & McCarthy method) with a minimum critical tilt angle of between 5° and 15° to move a 10 μl water droplet, but with no values reported for their advancing or receding contact angles[32].

Here we report experiments of the evaporation of sessile droplets of water on SOCAL coated glass surfaces with contact angle hysteresis of less than 1° over a range wide range of relative humidity (from 10% to 70%). In section 2.1 we describe preparation of SOCAL coatings with highly reproducible contact angles ~101°-105° and low contact-angle hysteresis $\Delta\theta_{CAH} \sim 1°$. In section 3, we report data showing the CCA mode evaporation for small sessile water droplets; we consistently measure contact angles close to the static values, and within the bounds expected from the measured and extremely low contact-angle hysteresis. In section 4, we discuss the entire evaporation sequence including a step change in the observed value of the constant contact angle that occurs at relative humidity between 30%

and 40%. Finally, we use the Picknett & Bexon model to analyze the evaporation of individual droplets and provide a set of estimates of the diffusion coefficient. By comparing the evaporation rate to the relative humidity across all experiments, we obtain a second estimate of the diffusion coefficient. Both types of estimate are within 2% of the literature value and show how SOCAL surfaces, which are omniphobic, provide a simple but accurate methodology to determine the diffusion coefficient of volatile liquids.

Experimental Method

SOCAL Preparation

Slippery Omniphobic Covalently Attached Liquid (SOCAL) surfaces were created on 25 × 75 mm glass slides using the method detailed by Wang & McCarthy adapted to our specific equipment and with process parameters iteratively developed until a reproducible and low contact angle hysteresis method was achieved[29]. Our optimized method used clean glass slides placed into a Henniker plasma cleaner (HPT-100) at 30% power for 20 minutes. This step adds OH bonds to the surface. The slide was then dipped into a reactive solution of isopropanol, dimethyldimethoxysilane and sulphuric acid (90, 9 and 1% wt.) for 5 seconds, then slowly withdrawn. The slides were then placed in a bespoke humidity-controlled environment at 60% relative humidity and 25 °C for 20 minutes. During this step, an acid-catalyzed graft polycondensation of dimethyldimethoxysilane creates a homogeneous layer of polydimethylsiloxane (PDMS) grafted to the surface. Unreacted material was then rinsed away with deionized (DI) water, isopropanol and toluene.

We found that to reliably produce SOCAL surfaces with low contact angle hysteresis, the following parameters need to be carefully controlled and optimized: plasma exposure time; the relative humidity at which the reaction takes place and the reaction time. With the plasma cleaner set to 100 W power and varying the treatment duration from 30 seconds to 30 minutes, we found a minimum in the contact angle hysteresis occurs at 5 minutes plasma time ($\Delta\theta_{CAH}$= 1.8 ± 0.7°). Although very low, this contact angle hysteresis is larger than previously reported by Wang & McCarthy[29]. By reducing the plasma power to 30 W, we were able to reduce the time sensitivity and achieve $\Delta\theta_{CAH}$=(0.9 ± 0.3°) with 20 minutes plasma cleaning time (Fig. 1). To assess the reproducibility and the uniformity of results across a surface, the contact angle hysteresis for each change in process parameter was assessed using advancing and receding contact angle measurements taken at three different locations on the surface; the average of the results across all three locations is reported with its standard deviation.

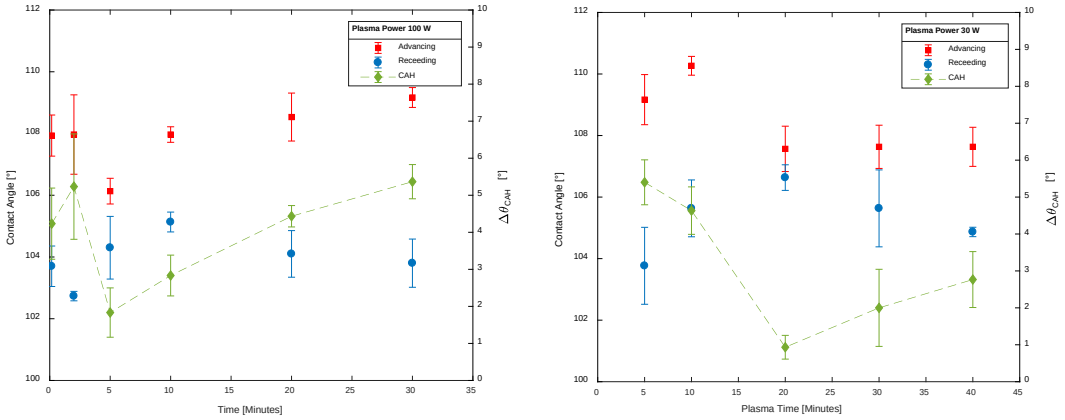

Figure 1: Contact angle hysteresis ($\Delta\theta_{CAH}$) as a function of plasma time. (Left) shows the $\Delta\theta_{CAH}$ as a function of time for 30 W plasma power. (Right) shows $\Delta\theta_{CAH}$ as a function of time for 100 W. The green dashed line is a guide to the eye.

Contact Angle Measurements

Contact angle measurements of droplets of water on the SOCAL surfaces were carried out using a Krüss drop shape analyzer (DSA 30) and Krüss DSA4 software. A 4 µL droplet of DI water was dispensed

onto the surface at room temperature (20 – 25 °C). A video sequence at 5 frames per second captured the inflation and deflation of the droplet to determine advancing and receding contact angles. The droplet was inflated by 2 μL at 20 μL/min, left to stabilize for 5 seconds then 2 μL was withdrawn at 1 μL/min. A slow withdrawal speed was used for contact angle hysteresis measurements to limit the risk that the measured angles were dynamic angles. In all reported measurements, the advancing angle, θ_A, is the angle immediately before the droplet radius begins to increase. Similarly, the receding angle, θ_R, is the angle immediately before the droplet radius begins to decrease. Each reported contact angle hysteresis value, $\Delta\theta_{CAH}=(\theta_A-\theta_R)$, is the average of contact angle hysteresis values measured at three different locations on the SOCAL treated glass slide.

Evaporation Experimental Procedure

Small (4.0 ± 0.3 μL) droplets of room temperature DI water (type III, purified in an Elga PURELAB® Option-Q lab water purification system) were deposited on a SOCAL treated glass slide, in a commercial humidity and temperature-controlled chamber (TC30) that had been equilibrated at (25 ± 0.1) °C, attached to a Krüss (DSA 25). The evaporation of the droplets was observed for a range of relative humidity from 10 to 70% (± 0.5%) in intervals of 10%. A further sequence of evaporation experiments refined the relative humidity range between 30% and 40% in steps of 2%. The evolution of the contact angle and the contact radius as a function of time were recorded using a Krüss drop shape analyzer (DSA 25), with time-lapse image capture at 10 second intervals (Fig. 2). The data and images for each evaporation sequence were analyzed individually to verify the absence of contact line pinning.

The contact radius was calculated by identifying the contact base-line by eye; the Krüss Advance software package then tracks the drop radius throughout the evaporation. The contact angle was evaluated using an elliptical fit in the Krüss Advance software, which uses the tangent of the ellipse intersecting the contact base-line. This gives a mean contact angle from the average of the left and right contact angle. Since SOCAL is a transparent coating, we were also able to confirm that droplets on the surfaces retained an axisymmetric shape during evaporation by conducting control experiments using simultaneous side profile and bottom up views.

Data presented in this paper shows typical curves for each relative humidity obtained from the average of three repeated evaporations. The data for each relative humidity was averaged into 100 equally spaced bins for each measured quantity (elapsed time, contact angle, contact radius). All of the experiments were carried out on five separately-made SOCAL treated glass slides at various locations on the slides. The different humidity experiments were carried out non-sequentially to ensure that no aging effects were observed.

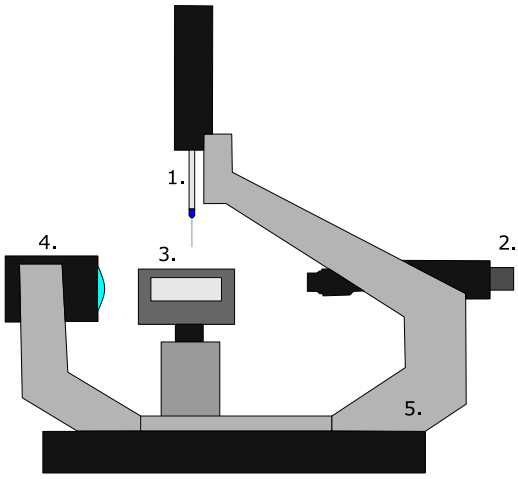

Figure 2: Diagram of experimental setup for evaporation. 1. Automatic syringe dosing unit. 2. Camera with macro lens and barrel. 3. Humidity and temperature controlled chamber (TC30). 4. LED backlight. 5. Krüss DSA 25.

Experimental Results

Typical Evaporation Sequence

Figure 3 shows the contact angle θ, and contact area, πr^2, as a function of time during a typical sessile droplet evaporation sequence. After short initial relaxation when a droplet is deposited, a constant contact angle is observed for the majority of the evaporation time. During the constant contact angle period the contact area reduces linearly with time. The short initial relaxation is likely to be due to the droplet equilibrating to the surface, temperature and relative humidity (e.g. see McHale *et al*[33]). The final stage of evaporation appears to be correlated to the observation of mineral deposit formation when the droplet radius reduced to ~0.5 mm, which is the radius at which the contact angle first begins to decrease.

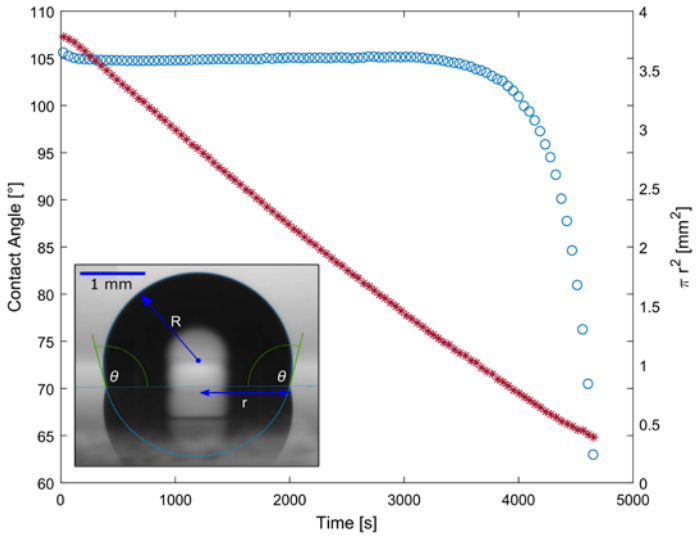

Figure 3: Typical evaporation showing contact angle (ooo) and contact area (***) as a function of time. The conditions of this typical evaporation are; a 4 µL droplet of DI water, 25 °C and 70% relative humidity. The insert shows the ellipse fitting of the droplet to measure the contact angle (θ) contact radius (r) and the spherical radius (R).

Influence of Relative Humidity

The constant contact angle mode of evaporation occurs across a broad range of relative humidity (10 – 70%. Figure 4 illustrates a typical evaporation at the lowest and highest values of relative humidity. Even though these extremes in relative humidity result in significantly different total evaporation times of 23 minutes and 2 hours 15 minutes, the droplet evaporation sequences demonstrate the same behavior. The presence of the syringe (seen at the top of each image in fig. 4) illustrates that an evaporating droplet remains centered, close its initial deposition location, from start to end of their evaporation. This provides confidence that the droplet contact line is completely mobile and free from pinning at all locations around the droplet.

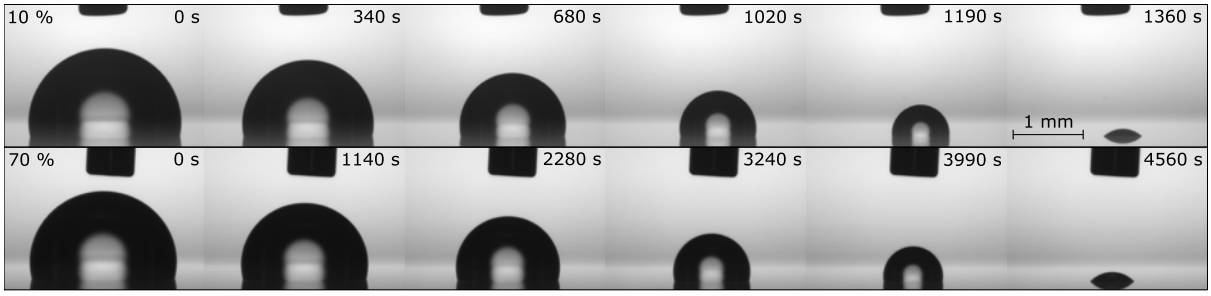

Figure 4: Evaporation time lapse at 10 and 70% relative humidity. The syringe needle is kept in the image to show the droplets evaporate moving radially inward in all directions.

Figure 5 shows a full set of sessile droplet evaporation sequences across the range of relative humidity from 10% to 70% in steps of 10% and using the volume as the horizontal axis to collapse all the data onto a single plot. The central inset in fig. 5 reveals that the constant contact angle during evaporation has two distinct values. The contact angle in the range of relative humidity of 10-30% is 101° whilst in the range of relative humidity of 30-40% there is a sharp rise in the constant contact angle to 104.5° which remains the value observed for the range from 40-70%. The step nature of this transition is further detailed in fig. 6, which presents data for the relative humidity range 30-40% using steps in relative humidity of 2%. Advancing angle measurements were carried out at each relative humidity value to confirm the surface retained low contact angle hysteresis despite this step change in contact angle. Evaporation causes the contact line to retreat slower than a needle withdrawing liquid therefore the receding angle at a given relative humidity is the angle observed during evaporation of liquid at that relative humidity. Contact angle hysteresis estimated using the constant receding angle during evaporation and the measured advancing contact angle prior to evaporation, was largest at RH=34% with $\Delta\theta_{CAH}$=(1.09 ± 0.27)° and lowest at RH=60% with $\Delta\theta_{CAH}$=(0.41 ± 0.16°). Figure 6 shows $\Delta\theta_{CAH}$ remains low for both contact angle regimes with $\Delta\theta_{CAH}$<2°.

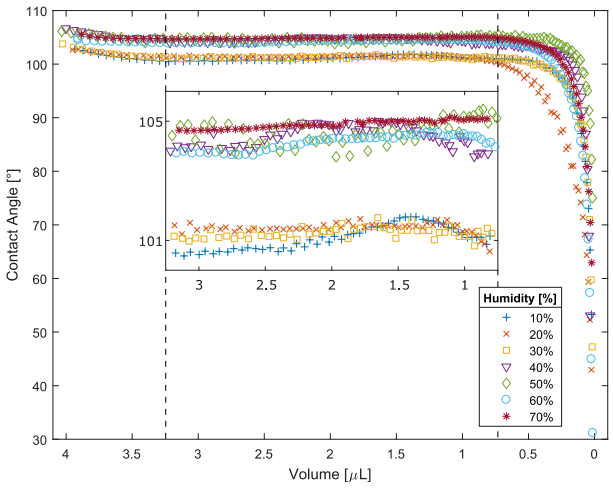

Figure 5: Contact angle as a function of volume. The dashed lines indicate the constant contact angle mode of evaporation. The central inset is a magnification of the CCA mode evaporation, showing the two contact angles for low (10-30%) and high (40-70%) relative humidity.

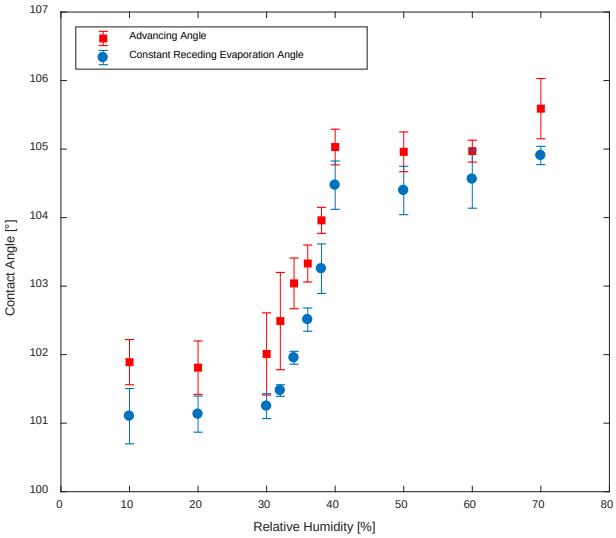

Figure 6: Step change in the value of the constant contact angle for evaporation at different relative humidity.

Analysis and Discussion

We first focus on the qualitative features of typical evaporation sequences. After a droplet is deposited, there is an immediate and short duration initial relaxation of the contact angle. The decrease in contact angle could be due to changes in temperature as evaporation establishes itself and evaporative cooling of the droplet and substrate occurs. For isolated evaporating spherical drops the cooling is determined by the evaporation rate[34] and this will also occur for sessile droplets with the evaporative cooling correlated to the relative humidity, which controls the rate of evaporation. In addition, thermal properties of the substrate will influence how effectively thermal energy can be supplied to maintain the temperature of the substrate surface. For example, Sefiane *et al.* show a link between the cooling effect on a droplet and the thermal properties of the substrate[35]. A further possibility is that evaporation creates a local relative humidity which, given the contact angle is over 90°, may be important for the precise value of contact angle due to the confined wedge space defined by the droplet and the substrate near the contact line. The simplest interpretation is that, although the contact angle hysteresis is very small, an evaporating droplet is simply adopting a receding contact angle which is slightly lower (1-2°) than its initial value on deposition.

The initial relaxation is then followed by a constant contact angle period that dominates the overall evaporation time. An unexpected feature in our data is the apparent separation into two distinct values of the constant contact angle of 101° and 104.5° for this constant contact angle evaporation mode. This step change for relative humidity between 30 and 40% is shown in fig. 6 and is reminiscent of the shape of a type V adsorption isotherm[36]. These two contact angle values can be compared to the 0.6° increase in contact angle hysteresis at the lower relative humidity values quantified using measurements *via* addition and withdrawal of liquid to a droplet. We excluded the step change being a consequence of a dynamic contact angle defined by the speed of retreat of the contact line by conducting receding contact angle measurement by withdrawal of liquid at different rates. We can also consider possible origins of the step change using Young's law (eq. 1) for which there are two interfacial tensions, γ_{LV} and γ_{SV}, that depend on the vapor. The first of these, the surface tension γ_{LV}, is known from pendant drop measurements to have a smooth change with temperature and relative humidity over the range used in our experiments (72.2 – 75.5 mN m^{-1}).[37,38] However, the second of these, the solid-vapor interfacial tension γ_{SV}, is a candidate for the origin of a step change in the observed contact angle. This might occur if a film of vapor condensed on the solid over the narrow 30-40% range of relative humidity thereby replacing the solid-vapor interface by solid-liquid and liquid-vapor interfaces. To consider this possibility we attempted to measure mass change on a SOCAL coated glass surface using a dynamic vapor sorption (DVS) method, but unfortunately it was not possible to obtain reliable results due to the small relative changes in mass. We also visually observed changes in reflectivity with relative humidity changes using a glass surface which had half of its area treated with the SOCAL coating, but did not observe any change indicating condensation had occurred. Another possibility is that the solid-vapor interfacial tension changes due to the adsorption of a monolayer of vapor. This could cause an increase in the contact angle as the relative humidity increases, as observed experimentally, due to increased cohesion of the water molecules and, hence, a decrease in the solid-vapor interfacial tension γ_{SV}. A further possibility, is that adsorption of a monolayer of water vapor could cause a step change in the mobility of the PDMS chains in the SOCAL coating for relative humidity above and below the 30-40% range. From these possibilities, vapor adsorption appears to be the most likely reason for the step change in contact angle with increasing relative humidity.

In the very final stages of evaporation the contact angle reduces rapidly and after the droplet had completely evaporated, we observed deposits were present over an area corresponding to that at which the contact angle first began to reduce. We therefore verified that the water we used did not contain solid particles. Energy dispersive X-ray spectroscopy (EDS) and scanning electron microscopy (SEM) Analysis of these deposits showed them to be composed of NaCl, AlCl, MgCl and KCl. This suggests

trace amounts of salts precipitated out of the water at a volume of 0.6 ± 0.1 μL and their deposition on the SOCAL-coated glass surface then created a self-pinning effect.

We now focus on a quantitative analysis of the evaporation sequences. Consider a sphere of liquid suspended in air far from any surface for which the rate of change in its volume due to diffusion-limited evaporation is given by

$$\frac{dV}{dt} = \frac{4\pi RD\Delta c}{\rho}, \tag{2}$$

where V is volume, R is the spherical radius of the droplet, D is the diffusion coefficient of water vapor in air, Δc is the difference between the vapour pressure close to the droplet and far away ($\Delta c = c_0 - c_\infty$), and ρ is the density of the liquid. Here the rate of change of volume arises from the net flux at the liquid-vapor interface integrated over the free surface of the droplet as discussed in the review by Cazabat and Guéna[12]. The same droplet resting on a solid surface, will adopt a spherical cap shape provided it is smaller than the capillary length, which for water is κ^{-1}=2.73 mm, and its contact area is not prevented by contact line pinning from adopting a circular shape. Geometrically this shape is defined by its contact angle, θ, with the surface and a contact radius r, as illustrated in the inset to fig. 3. Knowing these two parameters enables the volume of a spherical cap to be calculated using,

$$V = \frac{\pi}{3}\frac{(cos\theta - 1)^2(2 + cos\theta)r^3}{sin^3\,\theta} \tag{3}$$

Other geometrical parameters, such as the spherical radius, R, can also be calculated,

$$R = \left(\frac{3V}{\pi(2 - 3\cos\theta + cos^3\theta)}\right)^{1/3} \tag{4}$$

In addition to the change in droplet geometry from spherical to spherical cap, diffusion-limited evaporation is also influenced by the change in space into which vapor can diffuse. Thus, a completely spherical droplet with a contact angle of 180° just touching in flat solid surface does not evaporate as fast as a spherical droplet far from the surface. Picknett & Bexon considered sessile droplet evaporation and provided an exact closed-form solution for its diffusion-limited evaporation, which has a similar form to Eq. 2 but with an additional factor, $f(\theta)$, which is a function of the contact angle,

$$\frac{dV}{dt} = \frac{4\pi RD\Delta c}{\rho} f(\theta) \tag{5}$$

To aid numerical calculations, they provided polynomial fits to $f(\theta)$, covering the full contact angle range. For our experiments, the appropriate polynomial fit is for angles between $10° < \theta < 180°$ and is

$$f_{PB}(\theta) = \frac{1}{2}(0.00008957 + 0.6333\theta + 0.116\theta^2 - 0.8878\theta^3 + 0.01033\theta^4) \tag{6}$$

where θ is in radians. Since the droplets in our experiments conform to spherical caps, and unlike the work of Guan *et al.* on SLIPS[28] there is no wetting ridge present, these equations can be used directly to analyze our data. For the constant contact angle mode with side profile observations providing both contact angle and contact radius, the most appropriate equation arises by substituting eq. (3) into eq. (5) to give,

$$\frac{d(\pi r^2)}{dt} = \frac{8\pi D\Delta c\, sin^2\,\theta\, f_{PB}(\theta)}{\rho(cos\theta - 1)^2(2 + cos\theta)} \tag{7}$$

As the right-hand side of eq. (7) does not depend on time for the constant contact angle mode of evaporation, the contact area should reduce linearly with time.

Figure 7 shows representative data for sessile droplet evaporation on our SOCAL surfaces for each value of relative humidity (10-70%) and each can be seen to provide excellent agreement with a linear fit; the inset in fig. 7 illustrates the time range used to define the constant contact angle range. From the slopes in fig. 7, the diffusion coefficient for each relative humidity, D_{RH}, has been calculated using eq. (6) and is shown in table 1. These values of D_{RH} range from 2.31×10^{-5} m^2 s^{-1} to 2.87×10^{-5} m^2 s^{-1} with an average of $(2.58\pm0.20)\times10^{-5}$ m^2 s^{-1}, which compares well to the literature value of 2.48×10^{-5} m^2 s^{-1}. [39]

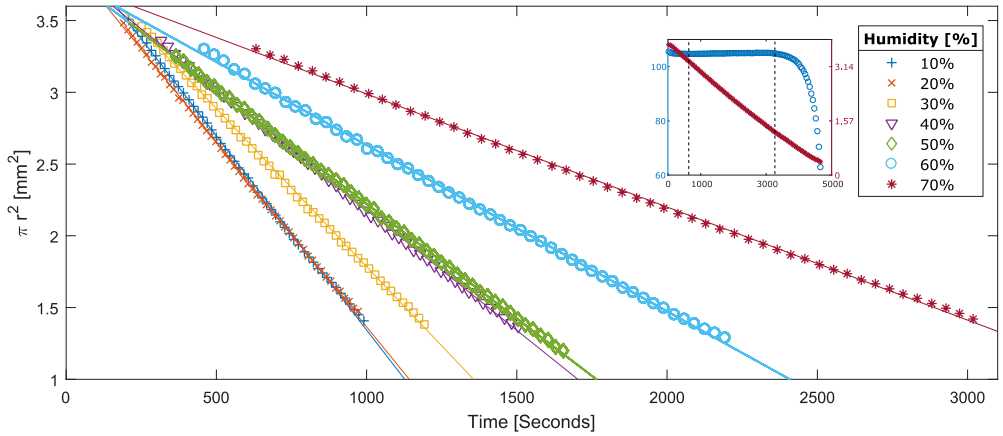

Figure 7: Contact area πr^2 as a function of time for evaporations at relative humidity 10-70%. The line through each data set represents the linear fit used to calculate D_{RH}. The inset shows the representative contact angle and contact area as a function of time, where the data between the dashed lines show the section of the evaporation that is CCA mode.

Relative Humidity [%]	$d\pi r^2/dt$ [mm^2 s^{-1}]	D_{RH} [x 10^{-5} m^2 s^{-1}]	D Literature [x 10^{-5} m^2 s^{-1}]
10	-0.002699	2.47	2.48
20	-0.002513	2.58	2.48
30	-0.002202	2.58	2.48
40	-0.001678	2.44	2.48
50	-0.001640	2.87	2.48
60	-0.001297	2.82	2.48
70	-0.000754	2.31	2.48
	Average:	**2.58 ± 0.20**	**2.48**

Table 1: Calculated diffusion coefficient for each relative humidity compared to the literature value.

Figure 7 provides confidence that we have observed constant contact angle mode evaporation, which is diffusion-limited, and table 1 confirms that the extracted diffusion coefficients from each relative humidity are consistent with the literature values. However, since the diffusion coefficient should not depend on the relative humidity, rearranging eq. (7) and relating the relative humidity RH to vapor concentration by $\Delta c = c_0((RH/100) - 1)$, allows a single estimated diffusion coefficient, D_E, to be calculated using all experiments across the range of relative humidity 10%-70%,

$$\frac{\rho(cos\theta - 1)^2(2 + cos\theta)}{8\pi\Delta c\, sin^2\theta\, f_{PB}(\theta)} \frac{d(\pi r^2)}{dt} = D_E \left(\frac{RH}{100} - 1\right) \quad (8)$$

Figure 8 shows data from fig. 7 plotted using eq. (7) and the gradient from this gives an estimate of the diffusion coefficient of D_E=(2.44 ± 0.48) x 10^{-5} m^2s^{-1}, which is an improved estimate compared to the single relative humidity estimates and which is within 2% of the literature value.

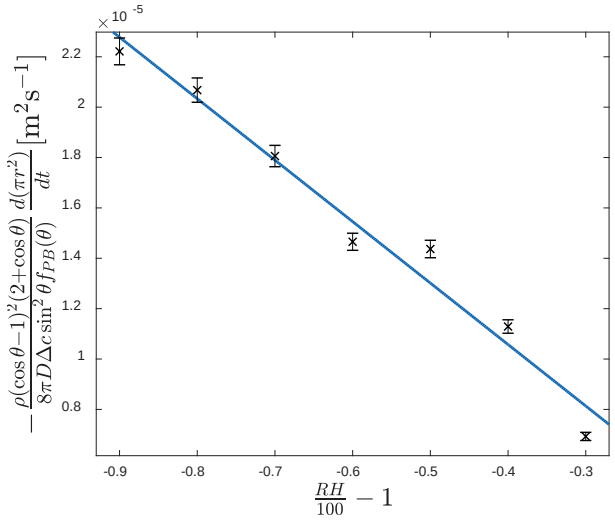

Figure 8: $d\pi r^2/dt$ as a function of relative humidity. The gradient of the plot gives the calculated diffusion coefficient D_E.

Finally, since Wang & McCarthy have reported that SOCAL surfaces are omniphobic and have low contact angle hysteresis to a wide range of liquids, including diiodomethane, toluene, hexadecane, cyclohexane, decane and hexane[29], the accuracy of our evaporation method of determining the diffusion coefficient for water suggests that a SOCAL coated glass surface could be used to determine the diffusion coefficients for a wide range of other liquids.

Conclusion

In this work, we have shown it is possible to observe the constant contact angle evaporation mode on a flat smooth (non-textured) solid surface by creating Slippery Omni-phobic Covalently Attached Liquid-like (SOCAL) coated surfaces with extremely low contact angle hysteresis. This differs from previous attempts to observe the CCA mode, which have relied on the use of textured solid surfaces, or a lubricant oil that removes all contact with a solid surface. We have also observed a step change in the constant contact angle value occurring in a narrow range of relative humidity (30-40%), which is indicative of the adsorption of water vapor on the surface and reminiscent of a type V isotherm. The value of the constant contact angle during evaporation has been shown to be consistent with the ideal contact angle from Young's law estimated by using independent measurements of the advancing and receding contact angle. Quantitative analysis of the sessile droplet evaporation sequences provides accurate measurements of the diffusion constant of the evaporating liquid. Hence, this methodology can provide a simple and reliable way to characterize the volatility of a wide range of other liquids.

Acknowledgements

The authors gratefully acknowledge Professor Chris Hardacre and Huan Xiang from the School of Chemical Engineering & Analytical Science, University of Manchester for assistance with DVS measurements and discussion of the results and Professor Doris Vollmer (Max Planck Institute for Polymer Research, Mainz) for discussions on the SOCAL method. RLA acknowledges support from EPSRC (Grant No. EP/P024408/1). SA would also like to acknowledge Dr. G Launay, Dr. E Ruiz-

Gutierrez, Dr. P Agrawal and H Barrio-Zhang for valuable advice and technical support. SA would also like to acknowledge Northumbria University at Newcastle for financial support.

References

(1) Erbil, H. Y. Evaporation of Pure Liquid Sessile and Spherical Suspended Drops: A Review. *Advances in Colloid and Interface Science*. **2012**, pp 67–86.

(2) Lim, T.; Han, S.; Chung, J.; Chung, J. T.; Ko, S.; Grigoropoulos, C. P. Experimental Study on Spreading and Evaporation of Inkjet Printed Pico-Liter Droplet on a Heated Substrate. *Int. J. Heat Mass Transf.* **2009**, *52* (1-2), 431–441.

(3) Li, T.; Xu, M.; Hung, D.; Wu, S.; Cheng, S. Understanding the Effects of Fuel Type and Injection Conditions on Spray Evaporation Using Optical Diagnostics. *SAE Tech. Pap.* **2015**, *2015-April* (March).

(4) Yuen, M. C.; Chen, L. W. Heat-Transfer Measurements of Evaporating Liquid Droplets. *Int. J. Heat Mass Transf.* **1978**, *21* (5), 537–542.

(5) Deegan, R. D.; Bakajin, O.; Dupont, T. F.; Huber, G.; Nagel, S. R.; Witten, T. A. Capillary Flow as the Cause of Ring Stains from Dried Liquid Drops. *Nature* **1997**, *389* (6653), 827–829.

(6) McHale, G. Surface Free Energy and Microarray Deposition Technology. *Analyst*. **2007**, pp 192–195.

(7) Frommelt, T.; Kostur, M.; Wenzel-Schäfer, M.; Talkner, P.; Hänggi, P.; Wixforth, A. Microfluidic Mixing via Acoustically Driven Chaotic Advection. *Phys. Rev. Lett.* **2008**, *100* (3), 1–4.

(8) Eral, H. B.; Augustine, D. M.; Duits, M. H. G.; Mugele, F. Suppressing the Coffee Stain Effect: How to Control Colloidal Self-Assembly in Evaporating Drops Using Electrowetting. *Soft Matter* **2011**, *7* (10), 4954–4958.

(9) Young, T. An Essay on the Cohesion of Fluids. *Philos. Trans. R. Soc. London* **1805**, *95*, 65–87.

(10) Picknett, R. G.; Bexon, R. The Evaporation of Sessile or Pendant Drops in Still Air. *J. Colloid Interface Sci.* **1977**, *61* (2), 336–350.

(11) Stauber, J. M.; Wilson, S. K.; Duffy, B. R.; Sefiane, K. On the Lifetimes of Evaporating Droplets with Related Initial and Receding Contact Angles. *Phys. Fluids* **2015**, *27* (12), 124102.

(12) Cazabat, A.-M.; Guéna, G. Evaporation of Macroscopic Sessile Droplets. *Soft Matter* **2010**, *6* (12), 2591.

(13) Larson, R. G. Transport and Deposition Patterns in Drying Sessile Droplets. *AIChE J.* **2014**, *60* (5), 1538–1571.

(14) Wong, T.-S.; Kang, S. H.; Tang, S. K. Y.; Smythe, E. J.; Hatton, B. D.; Grinthal, A.; Aizenberg, J. Bioinspired Self-Repairing Slippery Surfaces with Pressure-Stable Omniphobicity. *Nature* **2011**, *477* (7365), 443–447.

(15) Smith, J. D.; Dhiman, R.; Anand, S.; Reza-Garduno, E.; Cohen, R. E.; McKinley, G. H.; Varanasi, K. K. Droplet Mobility on Lubricant-Impregnated Surfaces. *Soft Matter* **2013**, *9* (6), 1772–1780.

(16) Cassie, A. B. D.; Baxter, S. Wettability of Porous Surfaces. *Trans. Faraday Soc.* **1944**, *40* (0), 546.

(17) Onda, T.; Shibuichi, S.; Satoh, N.; Tsujii, K. Super-Water-Repellent Fractal Surfaces. *Langmuir* **1996**, *12* (9), 2125–2127.

(18) Barthlott, W.; Neinhuis, C. Purity of the Sacred Lotus, or Escape from Contamination in Biological Surfaces. *Planta* **1997**, *202* (1), 1–8.

(19) Shirtcliffe, N. J.; McHale, G.; Atherton, S.; Newton, M. I. An Introduction to Superhydrophobicity. *Adv. Colloid Interface Sci.* **2010**, *161* (1-2), 124–138.

(20) McHale, G.; Aqil, S.; Shirtcliffe, N. J.; Newton, M. I.; Erbil, H. Y. Analysis of Droplet Evaporation on a Superhydrophobic Surface. *Langmuir* **2005**, *21* (24), 11053–11060.

(21) Wenzel, R. N. Resistance of Solid Surfaces to Wetting by Water. *Ind. Eng. Chem.* **1936**, *28* (8), 988–994.

(22) Zhang, X.; Tan, S.; Zhao, N.; Guo, X.; Zhang, X.; Zhang, Y.; Xu, J. Evaporation of Sessile Water Droplets on Superhydrophobic Natural Lotus and Biomimetic Polymer Surfaces. *ChemPhysChem* **2006**, *7* (10), 2067–2070.

(23) McLauchlin, M. L.; Yang, D.; Aella, P.; Garcia, A. A.; Picraux, S. T.; Hayes, M. A. Evaporative Properties and Pinning Strength of Laser-Ablated, Hydrophilic Sites on Lotus-Leaf-Like, Nanostructured Surfaces. *Langmuir* **2007**, *23* (9), 4871–4877.

(24) Tan, S.; Zhang, X.; Zhao, N.; Xu, J. Simulation of Sessile Water-Droplet Evaporation on Superhydrophobic Polymer Surfaces. *Chinese J. Chem. Phys.* **2007**, *20* (2), 140–144.

(25) Jung, Y. C.; Bhushan, B. Wetting Behaviour during Evaporation and Condensation of Water Microdroplets on Superhydrophobic Patterned Surfaces. *J. Microsc.* **2008**, *229* (1), 127–140.

(26) Kulinich, S. A.; Farzaneh, M. Effect of Contact Angle Hysteresis on Water Droplet Evaporation from Super-Hydrophobic Surfaces. *Appl. Surf. Sci.* **2009**, *255* (7), 4056–4060.

(27) Gelderblom, H.; Marín, Á. G.; Nair, H.; Van Houselt, A.; Lefferts, L.; Snoeijer, J. H.; Lohse, D. How Water Droplets Evaporate on a Superhydrophobic Substrate. *Phys. Rev. E - Stat. Nonlinear, Soft Matter Phys.* **2011**, *83* (2), 026306.

(28) Guan, J. H.; Wells, G. G.; Xu, B.; McHale, G.; Wood, D.; Martin, J.; Stuart-Cole, S. Evaporation of Sessile Droplets on Slippery Liquid-Infused Porous Surfaces (SLIPS). *Langmuir* **2015**, *31* (43), 11781–11789.

(29) Wang, L.; McCarthy, T. J. Covalently Attached Liquids: Instant Omniphobic Surfaces with Unprecedented Repellency. *Angew. Chemie - Int. Ed.* **2016**, *55* (1), 244–248.

(30) Jin, Y.; Zhang, L.; Wang, P. Atmospheric Water Harvesting: Role of Surface Wettability and Edge Effect. *Glob. Challenges* **2017**, *1* (4), 1700019.

(31) Mizutani, T.; Satake, U.; Enomoto, T. Surgical Diamond Wheels for Minimally Invasive Surgery in Bone Resection under Small Quantity of Coolant Supply. *Precis. Eng.* **2018**, *77*, 243–246.

(32) Daniel, D.; Timonen, J. V. I.; Li, R.; Velling, S. J.; Kreder, M. J.; Tetreault, A.; Aizenberg, J. Origins of Extreme Liquid Repellency on Structured, Flat, and Lubricated Hydrophobic Surfaces. *Phys. Rev. Lett.* **2018**, *120* (24), 244503.

(33) McHale, G.; Rowan, S. M.; Newton, M. I.; Banerjee, M. K. Evaporation and the Wetting of a Low-Energy Solid Surface. *J. Phys. Chem. B* **1998**, *102* (11), 1964–1967.

(34) Erbil, H. Y.; Dogan, M. Determination of Diffusion Coefficient-Vapor Pressure Product of Some Liquids from Hanging Drop Evaporation. *Langmuir* **2000**, *16* (24), 9267–9273.

(35) David, S.; Sefiane, K.; Tadrist, L. Experimental Investigation of the Effect of Thermal

Properties of the Substrate in the Wetting and Evaporation of Sessile Drops. *Colloids Surfaces A Physicochem. Eng. Asp.* **2007**, *298* (1-2), 108–114.

(36) Sing, K. S. W. Reporting Physisorption Data for Gas/solid Systems with Special Reference to the Determination of Surface Area and Porosity (Recommendations 1984). *Pure Appl. Chem.* **1985**, *57* (4), 603–619.

(37) Pérez-Díaz, J. L.; Álvarez-Valenzuela, M. A.; García-Prada, J. C. The Effect of the Partial Pressure of Water Vapor on the Surface Tension of the Liquid Water-Air Interface. *J. Colloid Interface Sci.* **2012**, *381* (1), 180–182.

(38) Portuguez, E.; Alzina, A.; Michaud, P.; Oudjedi, M.; Smith, A. Evolution of a Water Pendant Droplet: Effect of Temperature and Relative Humidity. *Nat. Sci.* **2017**, *09* (01), 1–20.

(39) Lide, D. R. *CRC Handbook of Chemistry and Physics: A Ready Reference Book of Chemical and Physical Data*; **1992**; Vol. 268.

Table of Contents/ Abstract Image